


AZGP1 Up-Regulation is a Potential Target for Andrographolide Reversing Radioresistance of Colorectal Cancer

Ye-Ying Fang¹, Jin-Mei Huang², Jia-Ying Wen¹, Jian-Di Li³, Jin-Hai Shen³, Da-Tong Zeng⁴, Yan-Fang Pan⁵, He-Qing Huang¹, Zhi-Guang Huang³, Li-Min Liu², Gang Chen³ 

¹Department of Radiation Oncology, the First Affiliated Hospital of Guangxi Medical University, Nanning, 530021, People's Republic of China;

²Department of Toxicology, College of Pharmacy, Guangxi Medical University, Nanning, 530021, People's Republic of China; ³Department of Pathology, the First Affiliated Hospital of Guangxi Medical University, Nanning, 530021, People's Republic of China; ⁴Department of Pathology, Red Cross Hospital of Yulin, Yulin City, 537000, People's Republic of China; ⁵Department of Pathology, Hospital of Guangxi Liugang Medical Co., LTD./Guangxi Liuzhou Dingshun Forensic Expert Institute, Liuzhou City, 545002, People's Republic of China

Correspondence: Gang Chen, 6#, Shuangyong Road, Nanning, 530021, People's Republic of China, Tel +86-771- 5356534, Fax +86-15277192134, Email chengang@gxmu.edu.cn

Background: Radiation resistance is a challenge that limits the therapeutic benefit of colorectal cancer (CRC) treatment, but the mechanism underlying CRC radiation resistance remains unclear. Andrographolide shows a broad-spectrum anti-tumor effect in various malignancies, including CRC, its effect and how it functions in CRC initiation, and radiation have not been established. This study aimed to explore the mechanism of CRC radiation resistance and the potential mechanisms of andrographolide on CRC radiation.

Methods: Two acquired radioresistant cell lines were established and high throughput sequencing was employed to screen out the differentially expressed genes. The expression of AZGP1, which was upregulated in the acquired radioresistant tissues, was verified by microarray data recomputing. The common targets of andrographolide, CRC initiation, and radiation resistance were obtained, and the corresponding functional enrichment and pathway analysis were performed. The interaction between AZGP1 and andrographolide was investigated using molecular docking.

Results: AZGP1 was upregulated in both the radioresistant cell model and microarray data. Moreover, AZGP1 was upregulated in cancerous colorectal tissue and displayed a tendency toward elevated expression in patients with an unfavorable prognosis. AZGP1 was identified as the common target of andrographolide, colorectal cancer initiation, and radiotherapy resistance. Ultimately, the protein structure of AZGP1 proved to be closely intertwined with the crystal texture of andrographolide.

Conclusion: AZGP1 is recognized as a crucial factor for both CRC initiation and radioresistance. Andrographolide may affect the radioresistance of CRC via the targeting of AZGP1. Thus, the combination of andrographolide and AZGP1 intervention might be a promising strategy for improving the treatment benefit of CRC radiotherapy.

Keywords: radiation resistance, colorectal carcinoma, AZGP1, alpha-2-glycoprotein 1, zinc-binding, andrographolide

Introduction

The incidence of colorectal cancer ranks third among all cancers worldwide, with rectal cancer accounting for about one third of cases.¹ Radiotherapy is an important method in the management of colorectal cancer. Neoadjuvant chemoradiation effectively increases the radical resection rate, reduces the risk of local recurrence, and facilitates an opportunity for anal sphincter-sparing.^{2,3} Postoperative adjuvant radiotherapy annihilates the subclinical residual tumor, reduces the postoperative recurrence rate, and ultimately improves treatment outcomes in terms of overall survival.⁴ Currently, neoadjuvant chemoradiotherapy followed by total mesorectal excision (TME) is the preferred therapeutic strategy for locally advanced rectal cancer.⁴ However, due to intrinsic heterogeneity, some tumors respond to radiation and benefit from radiotherapy, while some neoplasms are insensitive or even completely resistant to radiation. These radioresistant patients not only suffer from the adverse effects of radiation, but also endure a superfluous financial burden. A variety of biological factors contribute to

radiotherapy resistance, including hypoxia, anemia, and tumor necrosis. With the development of high-throughput sequencing, many expression profiles that are involved in radiotherapy resistance have been gradually revealed,⁵ but the specific molecular mechanism driving radiation resistance in rectal cancer remains unclear and needs to be further explored.

One strategy to overcome radiation resistance is the combination of drug sensitization. For example, cisplatin, etoposide, capecitabine, and fluorouracil have been widely used as radiation sensitization drugs in clinic.^{6,7} However, sensitization drugs have certain levels of toxicity, and their combination with radiotherapy inevitably leads to toxic accumulation, which limits the therapeutic outcomes.⁸ Therefore, the development of radiotherapy sensitizers with high efficiency and low toxicity would be promising for increasing radiotherapy sensitivity and improving the benefit of radiotherapy. Traditional Chinese medicine attracts extensive attention but has not been widely used in cancer treatment due to its mixed ingredients and a relative lack of evidence-based basis.⁹ In recent years, with the continuous development of the pharmacology of traditional Chinese medicine, many monomer components and action targets of traditional Chinese medicine have been gradually revealed, laying a foundation for its clinical application.

Andrographolide, the major bioactive compound isolated from *Andrographis paniculata* (Burm. f.) Nees, has been widely reported to possess diverse biological activities, such as anti-inflammation, anti-virus, anti-obesity, and anti-atherosclerotic activities.¹⁰ Andrographolide has broad-spectrum antitumor activity in colorectal,^{11–13} lung,¹⁴ breast,^{15,16} and head and neck cancers.¹⁷ It has been reported that andrographolide has a synergistic effect with various chemotherapeutics including carboplatin, capecitabine, 5-fluorouracil, thus improving the treatment effectiveness of laryngeal,¹⁷ colorectal,^{18,19} and lung cancer.²⁰ Andrographolide facilitates radiation-induced apoptosis or autophagy, thereby enhancing radiosensitivity in several experimental models. In a study conducted by Li et al, andrographolide sensitized HCT-116 colorectal cells to radiation by attenuating glycolysis.²¹ However, the precise mechanism of andrographolide on radiation remains to be explored.

In this study, to elucidate the molecular mechanism of radiotherapy resistance in colorectal cancer, we investigated the crucial genes being involved in colorectal cancer radiation resistance. The potential mechanism of andrographolide in colorectal cancer was also excavated. AZGP1 was identified as the potential target of andrographolide reversing radiation resistance of CRC, and its clinical value was explored. The current study may help to elucidate the molecular mechanism of colorectal cancer initiation and radiotherapy resistance, and furnish novel therapeutic strategy for radiation resistance.

Materials and Methods

The Establishment of Radioresistant CRC Cell Lines and Transcription Profile Analyses

Human colorectal cancer cell lines CX-1 and HCT-116 were purchased from the National Collection of Authentic Cell Cultures (Shanghai, China) and conventionally cultured in DMEM (Gibco, Waltham, MA, USA) in a humidified incubator at 37°C. To establish radioresistant cell lines, CX-1 and HCT-116 parental cells received 4Gy of photon beam radiation twice a week in an X-RAD225 cell and small animal x-ray irradiation (Precision X-Ray, North Branford, USA), with an accumulated dose of 80Gy. To validate the radiation resistance, plate clone formation assay was conducted to detect the surviving fraction, flow cytometry was employed to determine cell cycle, and apoptosis was detected using Annexin V-EGFP Apoptosis Detection Kit and Propidium Iodide (PI) Detection Kit (KeyGen, Nanjing, China) each according to the manufacturer's procedures.

The Expression Profile Analyses

Total RNA was harvested using Trizol reagent (Invitrogen, Carlsbad, CA, USA), according to the manufacturer's instructions. NanoDrop2000 (Thermo Fisher Scientific, Massachusetts, US) was used to measure the concentration and purity of the isolated RNAs. An RNA Removal Kit (Illumina, San Diego, USA) was employed to remove ribosomal RNA, and the remaining RNAs were fragmented into small pieces. The first-strand cDNAs were reverse-transcribed from the RNA fragments and then synthesized into U-labeled, second-strand DNAs with E. coli DNA polymerase I, DNase H, and dUTP. A two-step PCR was performed to ligate and amplify the synthesized cDNAs. Ultimately, an Illumina HiSeq 4000 (LC Bio, Hangzhou, China) was utilized to conduct paired-end sequencing according to the vendor's directions. Sequence quality control was performed using FastQC, an open-sourced Java program developed for sequencing quality assessment. The expression values of mRNAs were quantified by calculating FPKM values using StringTie. The differentially expressed

mRNAs were filtered by edge R package, and the genes with both \log_2 (fold change) >1 and p value < 0.05 were considered radioresistance-related genes.

Screening Radioresistance-Related Genes from GEO and ArrayExpress Databases

CRC-associated microarrays were searched for in the GEO (<http://www.ncbi.nlm.nih.gov/geo/>)²² and ArrayExpress databases (<https://www.ebi.ac.uk/arrayexpress/>)²³ on December 1, 2020. The following terms were used: [“Rectal” OR “Colorectal” MeSH] AND [“Neoplasms” OR “Neoplasm” MeSH Terms]. For the search for radiotherapy-associated microarrays, an additional term was employed: [“chemoradiotherapy” OR “radiation therapy” OR “radiotherapy” OR “radiation treatment” OR “irradiation” or “radiation” MeSH]. The inclusion criteria were: The sample sizes were greater than 3 per group; mRNA expression was quantifiable; and the samples were human CRC tissue or CRC cell lines. The detailed information from each radiotherapy-related microarray dataset was screened and extracted. The radiosensitivity of CRC tissue was assessed by the tumor regression scoring of NCCN guideline V2018,⁴ in which a TRG score of 0 was defined as radiosensitive, while a score between 1 and 3 was radioresistant. To screen out radioresistance-related genes, the CRC datasets from GEO or ArrayExpress were \log_2 transformed. To eliminate batch effects, the datasets from the same detecting platform were merged using the ComBat algorithm of the sva R package.²⁴ The processed datasets were computed for standard mean difference (SMD) in batches using meta-R package. The genes with an SMD absolute value of more than 0 and a p value of less than 0.05 were regarded as differentially expressed genes; those upregulated in the radioresistant group were intersected with radioresistant genes acquired from in-house high-throughput sequencing. AZGP1 was selected for further analysis because it was upregulated both in radioresistant groups of GEO datasets and the acquired radioresistant cells. There were no human participants or animals being involved in this study, informed consent for specimen usage was waived.

Verification of the Upregulation of AZGP1 in Radioresistant Tissue and Cancerous Tissue

To verify the upregulation of AZGP1 in radioresistant tissue, the expression values of AZGP1 were obtained from each dataset. After removing the batch effects, the expression of AZGP1 in each dataset was visualized by boxplots, using the ggplot2 R package. To investigate the power of AZGP1 to discriminate between radiosensitive and radioresistant tissue, we used the pROC R package to generate receiver operating characteristic curves (ROC), and the area under the curve (AUC) quantified the discrimination between individual groups. To enable a direct comparison between different detection platforms, the expression values were pooled into a continuous variable meta-analysis in Stata 15.0 software to calculate the SMD, and the results were visualized in the form of forest plots. An χ^2 test of Q and an I^2 statistic were performed to detect heterogeneity across studies. The values $p \geq 0.05$ and $I^2 \leq 50\%$ indicated no existence of heterogeneity, in which case a conditional fixed-effects model was employed; otherwise, a random fixed-effects model was applied. A linear regression model (Begg's test) was applied to examine the publication bias. Subsequently, a diagnostic meta-analysis was performed, and the specificity, sensitivity, positive likelihood ratio (LR), negative LR, diagnostic odds ratio (OR), and the summarized ROC were obtained. The differential expression of AZGP1 in cancerous and normal colorectal tissue was calculated in the same way.

The Expression of AZGP1 at the Protein Level

The Human Protein Atlas (THPA) (<https://www.proteinatlas.org/>),²⁵ an open-source database that includes the expression profiles of various proteins in human tissues was searched. Immunohistochemical staining of AZGP1 protein in CRC tissue and normal colorectal tissue was subsequently employed to display the differential expression of AZGP1.

The Prognostic Value of AZGP1 in CRC Patients

To determine the impact of AZGP1 expression on the prognosis of CRC patients, gene expression profiling interactive analysis (GEPIA) (<http://gepia.cancer-pku.cn/>)²⁶ was used, following the default setting of the database. The prognoses were categorized as overall survival (OS) and disease-free survival (DFS), and the corresponding survival curves were generated.

Collection of Potential Targets for Andrographolide in the Treatment of Radioresistance of Colorectal Carcinoma

The targets of andrographolide were obtained using the Traditional Chinese Medicine Systems Pharmacology (TCMSP),²⁷ Drugbank, SuperPred, and Swiss Target Prediction databases, following the default instructions. The overlapping genes from potential targets of andrographolide and CRC radioresistance-related genes were recognized as the target of andrographolide reversing radioresistance in CRC.

Functional Enrichment and Pathway Analysis

To reveal the biological characteristics of the putative target genes, gene ontology (GO) and Kyoto Encyclopedia of Genes and Genomes (KEGG) enrichment analyses were both performed using the ClusterProfiler R package with the default setting. The R package ggplot2 was employed to display the enrichment results.

Molecular Docking

Molecular docking of andrographolide and AZGP1 were conducted using SYBYL-X 2.1.1 software to verify their interaction activity. The SYBYL-X 2.1.1 software evaluated the binding quality of small molecules to proteins, primarily through the total score. A score greater than 6 indicated that the ligand and the receptor could spontaneously bind, and a higher value indicated that the active component bound to the receptor more easily. At present, no unified standard for the screening of active molecules using SYBYL-X is available. A review of the literature found that the docking conducted in this study showed good results.

Statistics Analysis

For a comparison of AZGP1 expression in individual datasets, a group *t*-test was conducted, and the values of AZGP1 were displayed as box plots using the ggplot2 R package. The corresponding ROCs were generated to reveal the discriminating power of AZGP1 in CRC cancerous samples versus normal tissue. To determine the impact of AZGP1 on the prognosis of CRC, rank logic was employed to compare the DFS and OS of patients with high or low AZGP1 expression. In this study, $p < 0.05$ was considered statistically significant.

Results

The Flow Diagram in Figure 1 Shows the General Design of the Study

Briefly, the acquired radioresistant cell lines were generated, and high-throughput sequencing and comprehensive microarray data-mining were conducted to screen out radioresistance-related genes. After AZGP1 was screened out, its expression in CRC tissue or cells with discrepant radiosensitivity was calculated and visualized. Then the upregulation of AZGP1 in CRC tissue was confirmed by a SMD calculation, and its influence on the prognosis of CRC was investigated. Finally, the interaction of AZGP1 with andrographolide was investigated, and molecular docking was conducted.

AZGP1 Was Upregulated in Acquired Radio-Resistant Cells

After repeated radiation exposure, two radioresistant cell lines (namely HCT-116-R and CX-1-R), which were derived from HCT-116 and CX-1, were established. HCT-116-R and CX-1-R cells showed resistance to radiation, compared with the corresponding parental cells. Specifically, the cell apoptosis ratio declined, while the proportion of cell survival and the G2/M phase cell-cycle arrest increased (unpublished data). In comparison with the corresponding parental cell lines, there were 51 and 37 genes upregulated in HCT-116-R and CX-1-R, respectively. The downregulation of 47 and 61 genes were observed in HCT-116-R and CX-1-R, respectively ([Supplemental Table 1](#)). The volcano plots of the differentially expressed genes are shown in [Figure 2](#). After taking the intersection, two upregulated genes (GPX1, AZGP1) and three downregulated genes (HSPA8, PYCR1, MORF4L2) remained. Alpha-2-glycoprotein 1, zinc-binding (AZGP1), was upregulated in both HCT-116-R and CX-1-R cell lines, with a fold change value of log2 (fold change) of 1.22 and

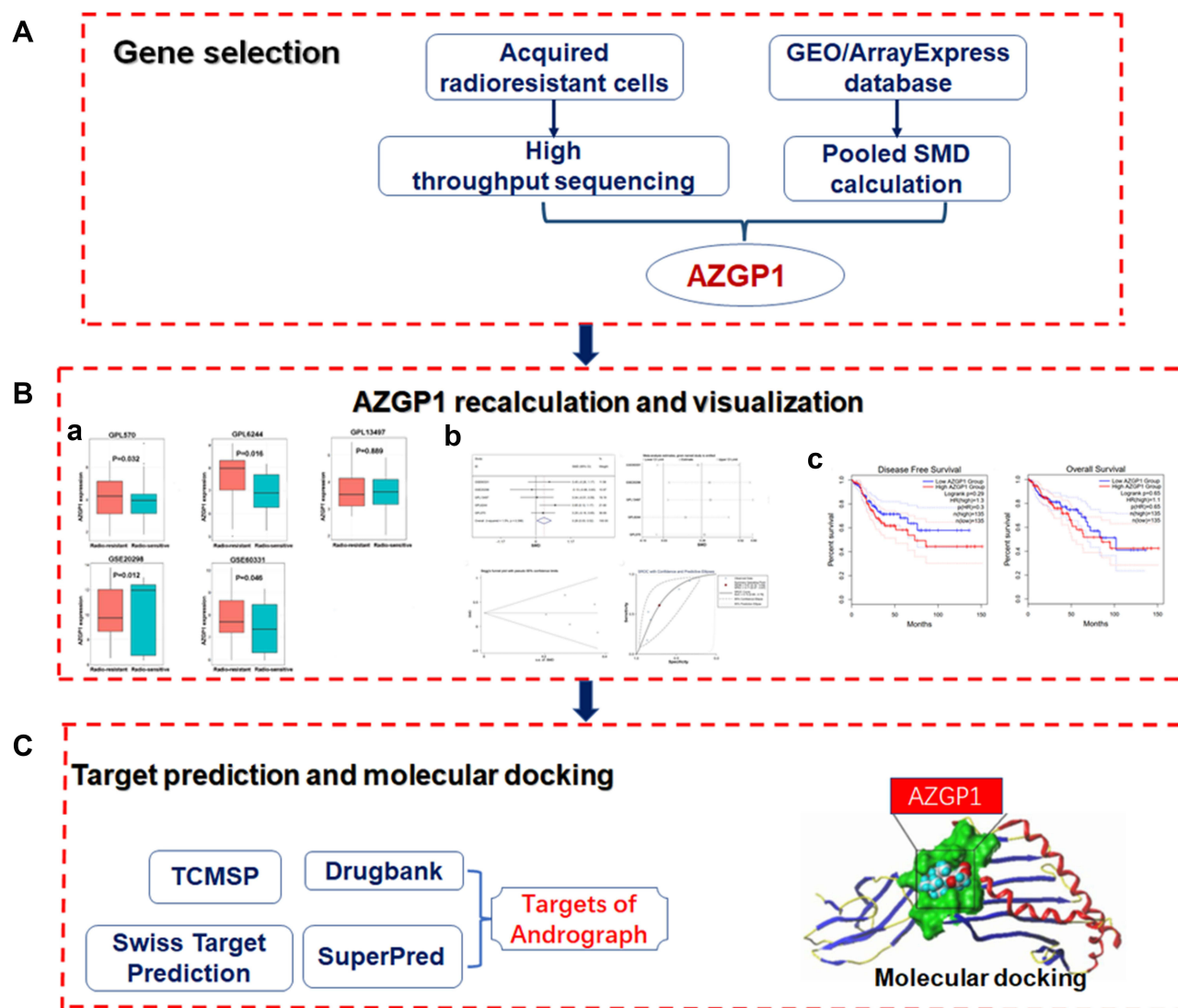


Figure 1 Flow diagram of the study design. **(A)** The procedure of selecting AZGP1 as the key gene. **(B)** AZGP1 expression in rectal samples and its visualization; (a) Box plots of AZGP1 differential expression in radioresistant and radiosensitive CRC samples; (b) The integrated SMD and diagnostic meta-analysis of AZGP1 expression in radioresistant versus radiosensitive CRC samples; (c) Survival analysis in patients with CRC in terms of disease-free survival and overall survival. **(C)** Target prediction for andrographolide and molecular docking. GEO, Gene Expression Omnibus database; SMD, standard mean difference; TCMSP, traditional Chinese medicine systems pharmacology.

1.37, respectively. The results of GO and KEGG enrichment analyses on differential expressed genes in the radioresistant cellular model are displayed in [Supplemental Figure 1](#).

AZGP1 Was Upregulated in Radioresistant CRC Tissue and Cells

Based on the pooled SMD computing, there were 155 genes upregulated in CRC tissue with radiation resistance, while 169 downregulated genes were detected. AZGP1, which was upregulated in the acquired radioresistant cells, was also among the 155 upregulated genes, with a SMD value of 0.268 ($p = 0.03$). We then recomputed the expression of AZGP1 in individual datasets. Among eight microarray datasets from five platforms ([Supplemental Table 2](#)), AZGP1 was upregulated in three platforms, including GPL570 ([Figure 3A](#)), GPL6244 ([Figure 3B](#)) and GSE60331 ([Figure 3E](#)), while a downregulation of AZGP1 was observed in the radioresistant group of the GSE20298 dataset ([Figure 3D](#)). No difference in AZGP1 expression was found between the radioresistant and the radiosensitive cells in the GPL13497 platform ([Figure 3C](#)). As the ROC curves show in [Figure 4](#), the AUC of each dataset was 0.579 (GPL570) ([Figure 4A](#)), 0.704 (GPL6244) ([Figure 4B](#)), 0.527 (GPL13497) ([Figure 4C](#)), 0.568 (GSE20298) ([Figure 4D](#)), and 0.617 (GSE60331) ([Figure 4E](#)). Since the expression pattern of AZGP1 was

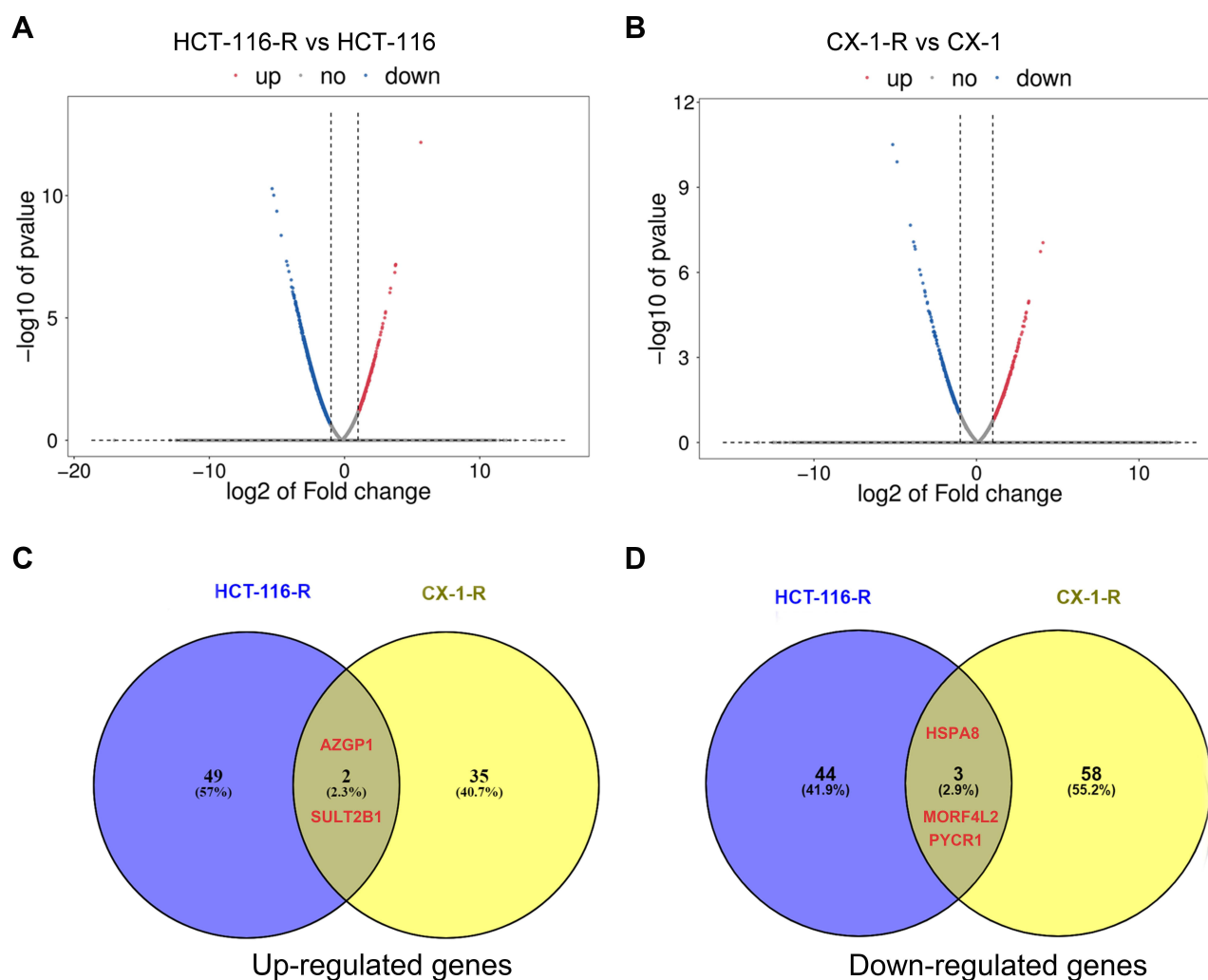


Figure 2 Differentially expressed genes in the acquired radioresistant colorectal cell lines. **(A)** volcano plots displaying the differentially expressed genes in HCT-116-R cells and HCT-116 cells. **(B)** volcano plots of the differentially expressed genes in CX-1-R cells versus CX-1 cells. The dark red dots represent the upregulated genes, the deep-blue dots represent the downregulated genes, and the gray dots represent genes with no differential expression. **(C)** Venn diagrams displaying the upregulated genes in HCT-116-R cells and CX-1-R cells. **(D)** Venn diagrams displaying the downregulated genes in HCT-116-R cells and CX-1-R cells.

not consistent across platforms, a continuous variable meta-analysis was performed, and the SMD value of AZGP1 was calculated. AZGP1 expression is illustrated in forest plots, with a SMD value of 0.28 (95% CI, 0.03–0.52) (Figure 5A). The forest plot in Figure 5B indicated no existence of heterogeneity. The funnel plots revealed no publication bias in this analysis model ($p > 0.05$, Figure 5C). The AUC value of the sROC was 0.72 (95% CI, 0.68–0.76, Figure 5D). The pooled sensitivity, specificity, positive likelihood ratio (PLR), negative likelihood ratio (NLR), and diagnostic odds ratio (DOR) were 0.61 (95% CI, 0.32–0.84), 0.78 (95% CI, 0.47–0.87), 2.11 (95% CI, 1.41–3.16), 0.55 (95% CI, 0.32–0.95), and 3.84 (95% CI, 1.98–3.47) (Supplemental Figure 2).

AZGP1 Was Upregulated in CRC Tissue and Correlates with Poor Prognosis

To investigate whether AZGP1 is involved in the initiation of CRC, the expression of AZGP1 in normal colon tissue and CRC tissue was compared in 23 datasets from 17 detecting platforms (Supplemental Table 3). As shown in Figure 6, AZGP1 was elevated in CRC tissue, except for in the GSE28000 (Figure 6H) and GSE141174 datasets (Figure 6O). The discriminative value of AZGP1 was satisfactorily high, as the AUC values shown in Figure 7A–Q, were 0.846 (95% CI, 0.803–0.838) (GPL96), 0.930 (95% CI, 0.893–0.968) (GPL10558), 0.954 (95% CI, 0.907–1.000) (GPL15207), 0.598 (95% CI, 0.413–0.782) (GSE15781), 0.970 (95% CI, 0.930–1.000) (GSE20842), 0.861 (95% CI, 0.749–0.973)

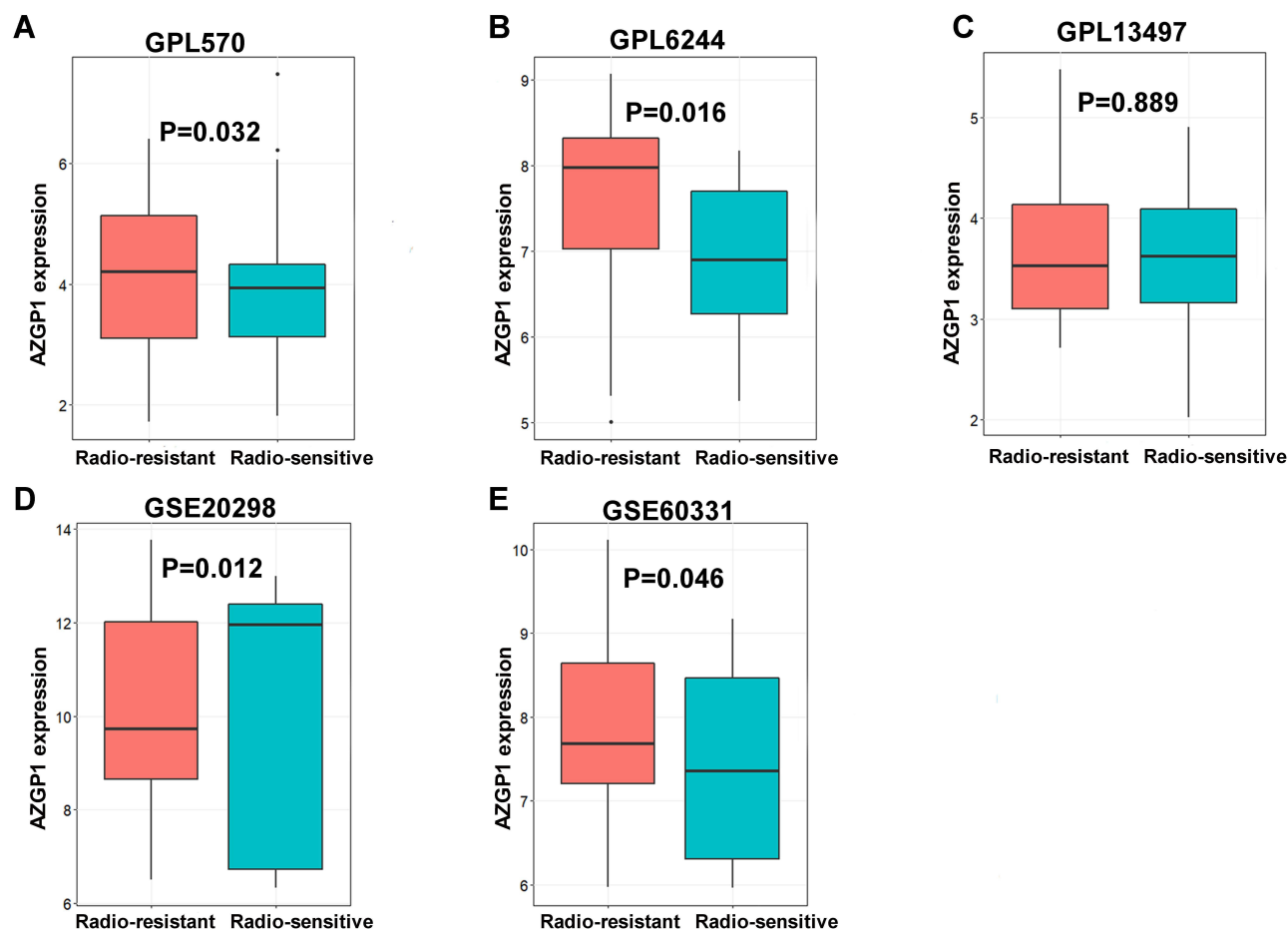


Figure 3 Box plots of AZGP1 differential expression in radioresistant and radiosensitive CRC samples. (A) GPL570 platform containing data from GSE35452 and GSE119409 series; (B) GPL6244 platform containing data from GSE43206 and GSE46862 series; (C) GPL13497 platform containing data from GSE97543 and GSE150082 series; (D) GSE20298 dataset; (E) GSE60331 dataset. The Orange boxes represent the expression of AZGP1 in radioresistant samples, while the turquoise boxes represent the expression of AZGP1 in radiosensitive samples.

(GSE24713), 0.940 (95% CI, 0.867–1.000) (GSE25071), 0.600 (95% CI, 0.224–0.976) (GSE28000), 0.958 (95% CI, 0.926–0.989) (GSE44076), 0.929 (95% CI, 0.789–1.000) (GSE47063), 0.939 (95% CI, 0.911–0.968) (GSE87211), 0.835 (95% CI, 0.694–0.976) (GSE103512), 0.949 (95% CI, 0.874–1.000) (GSE113513), 0.950 (95% CI, 0.847–1.000) (GSE115261), 0.556 (95% CI, 0.000–1.000) (GSE141174), 1.000 (95% CI, 1.000–1.000) (GSE156355), and 0.930 (95% CI, 0.910–0.949) (TCGA+CTEx). To directly compare data from different platforms, the SMD was calculated. In comparison with normal colorectal tissue, AZGP1 was upregulated in CRC tissue, with a SMD value of 1.87 (95% CI, 1.480–2.250) in the random effect model (Figure 8A). The forest plot for sensitivity analysis is shown in Figure 8B, and no heterogeneity was detected. The funnel plot revealed no publication bias in this integrative computation ($p > 0.05$; Figure 8C). An AUC value of 0.95 (95% CI, 0.92–0.97) substantiated the distinguishing power of AZGP1 (Figure 8D). The pooled sensitivity, specificity, PLR, NLR, and DOR were 0.95 (95% CI, 0.90–0.98), 0.86 (95% CI, 0.80–0.90), 17.18 (95% CI, 8.31–35.52), 0.15 (95% CI, 0.11–0.22) and 112.78 (95% CI, 43.82–290.27), respectively (Supplemental Figure 3). We then determined the expression of AZGP1 at the protein level. AZGP1 protein was detected in the cytoplasm and membrane of rectal carcinoma. In contrast, no AZGP1 staining was observed in normal small-intestine tissue, normal colon tissue, or normal rectum tissue (Figure 9). According to GEPIA, AZGP1 showed a tendency to negatively impact the prognosis of CRC patients in terms of disease-free survival. Patients with low AZGP1 expression had a better disease-free survival than those with high AZGP1 expression, though the difference was not statistically significant ($p=0.3$) (Figure 10A). In terms of overall survival, the AZGP1 expression has no impact ($p=0.65$) (Figure 10B).

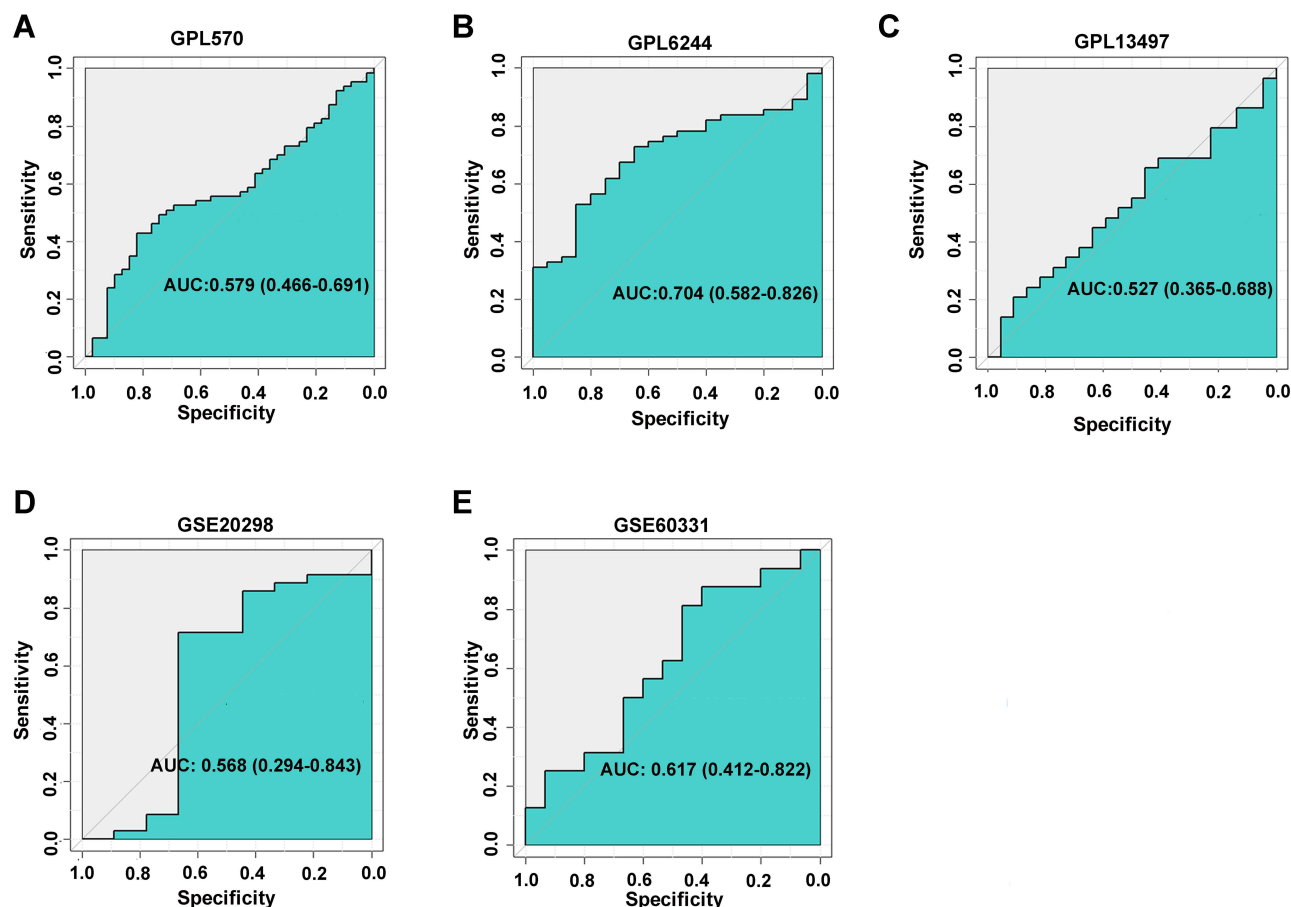


Figure 4 Corresponding ROC curves of AZGP1 differentiated expression in radioresistant versus radiosensitive CRC samples. **(A)** GPL570 platform containing data from GSE35452 and GSE119409 series; **(B)** GPL6244 platform containing data from GSE43206 and GSE46862 series; **(C)** GPL13497 platform containing data from GSE97543 and GSE150082 series; **(D)** GSE20298 dataset; **(E)** GSE60331 dataset.

Andrographolide May Alleviate Radioresistance of CRC via Targeting of AZGP1

As mentioned above, there were 155 genes upregulated in radioresistant colorectal cells, while 874 genes were upregulated in CRC tissue, based on the pooled SMD calculation. After taking the intersection, 19 genes remained, including AZGP1, CD55, CLDN1, DACH1, DPEP1, FAM84B, GAS2, KLK6, KRT23, LCN2, PTPN12, S100P, SFTA2, SP5, SULT2B1, TACSTD2, TBC1D4, TMPRSS3, and TNFRSF11B. There were 209 potential targets of andrographolide from multiple databases and text mining, including two genes that overlapped with the abovementioned 19 genes, including AZGP1 and SULT2B1 (Figure 11). The targets of andrographolide were then subjected to GO enrichment analysis, and the top 10 terms were response to steroid hormone, cellular response to steroid hormone stimulus, steroid metabolic process, response to peptide, hormone-mediated signaling pathway, steroid hormone-mediated signaling pathway, regulation of lipid metabolic process, response to molecule of bacterial origin, and extrinsic apoptotic signaling pathway (Figure 12A). For KEGG, the top 10 enriched pathways were Th17 cell differentiation, the AGE-RAGE signaling pathway in diabetic complication, the C-type lectin receptor signaling pathway, hepatitis B, tuberculosis, prostate cancer, osteoclast differentiation, t-cell receptor signaling pathway, thyroid hormone signaling pathway, and Yersinia infection (Figure 12B). Because AZGP1 was not only upregulated in cancerous colorectal tissue and radioresistant rectal tissue, but also the potential targets of andrographolide, molecular docking between AZGP1 and andrographolide was conducted. As the schematic diagram in Figure 13 shows, the protein structure of AZGP1 was closely intertwined with the crystal texture of andrographolide, with a total score of 7.0941.

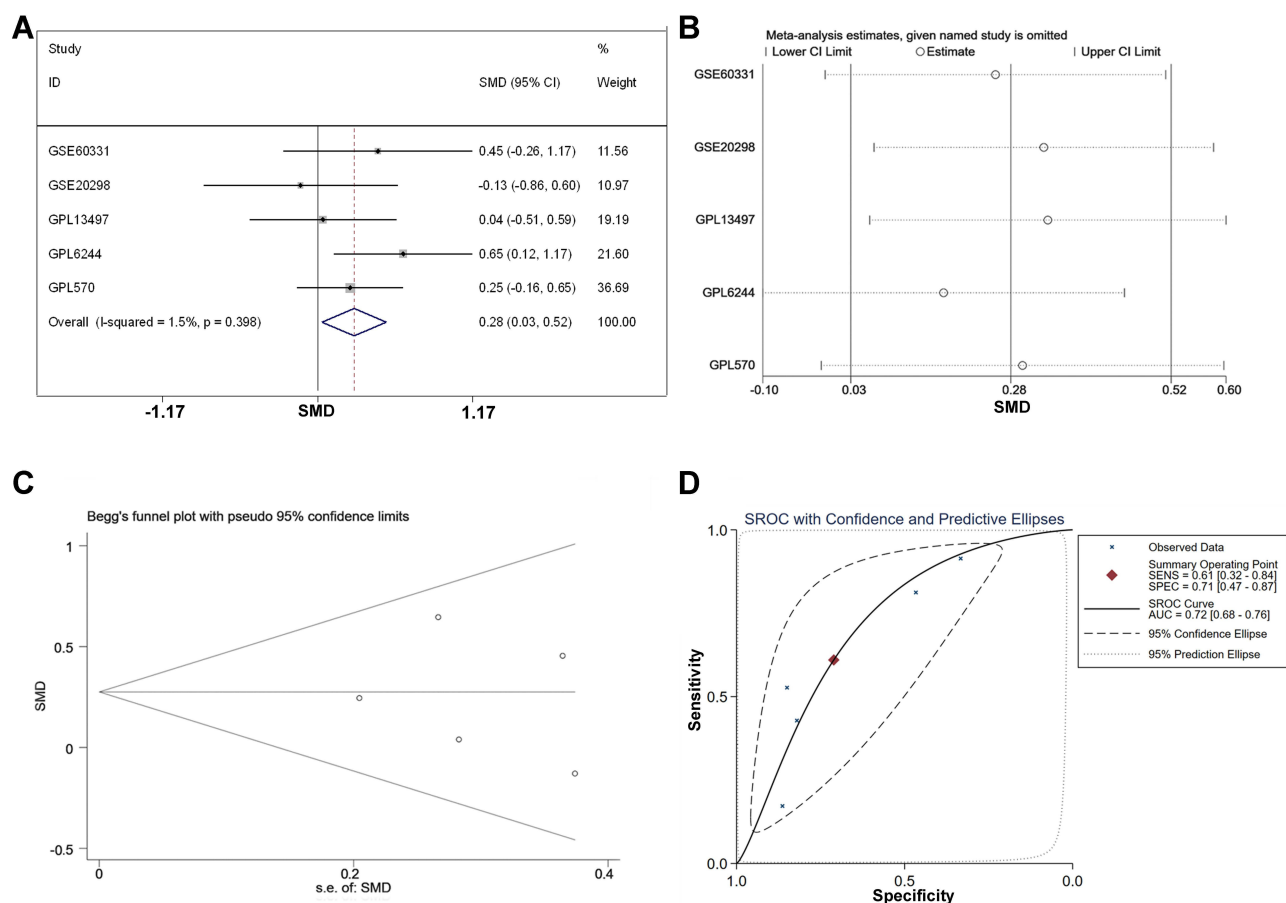


Figure 5 The integrated SMD and diagnostic meta-analysis of AZGP1 expression in radioresistant versus radiosensitive CRC samples. **(A)** forest plots of SMD values; **(B)** forest plot of sensitivity analysis; **(C)** funnel plot; **(D)** SROC curve of all included studies.

Discussion

In the present study, we established two colorectal cancer cell lines with acquired radioresistance and found that AZGP1 was upregulated in the radioresistant cell model by high-throughput transcriptome sequencing. Subsequently, the upregulation of AZGP1 in radioresistant CRC tissue was confirmed with microarray data. In addition, AZGP1 was upregulated in colorectal cancerous tissue, in comparison with normal colon tissue, with an appreciable discriminability. AZGP1 displayed a tendency toward elevated expression in patients with an unfavorable prognosis. Through target prediction and text mining, AZGP1 was identified as the common target of andrographolide, colorectal cancer initiation, and radiotherapy resistance. Ultimately, the protein structure of AZGP1 was closely intertwined with the crystal texture of andrographolide.

Due to improvements in treatment modalities and cancer screening, the last two decades have seen a decrease in the incidence rate and mortality of colorectal cancer.¹ Preoperative chemoradiation followed by total mesentery excision (TME) and adjuvant chemotherapy has been established as the standardized treatment pattern for local advanced rectal cancer.² Some patients are not suitable for TME due to advanced age or cardiovascular pulmonary diseases, thus a “wait and watch” approach after pelvic radiation is applicable for some patients.²⁸ Radiation resistance, however, limits the therapeutic outcomes and necessitates an understanding of its underlying mechanism.

It was conventionally believed that radiation resistance was a spontaneous phenomenon and that intrinsic genetic variation played an essential role in this biological process. However, intrinsic genetic variation could not fully explain the generation of radiation resistance. Actually, repeated exposure to x-rays or drugs also attenuates the response of tumors to radiation and chemotherapy, which subsequently leads to worse local control and even unfavorable treatment

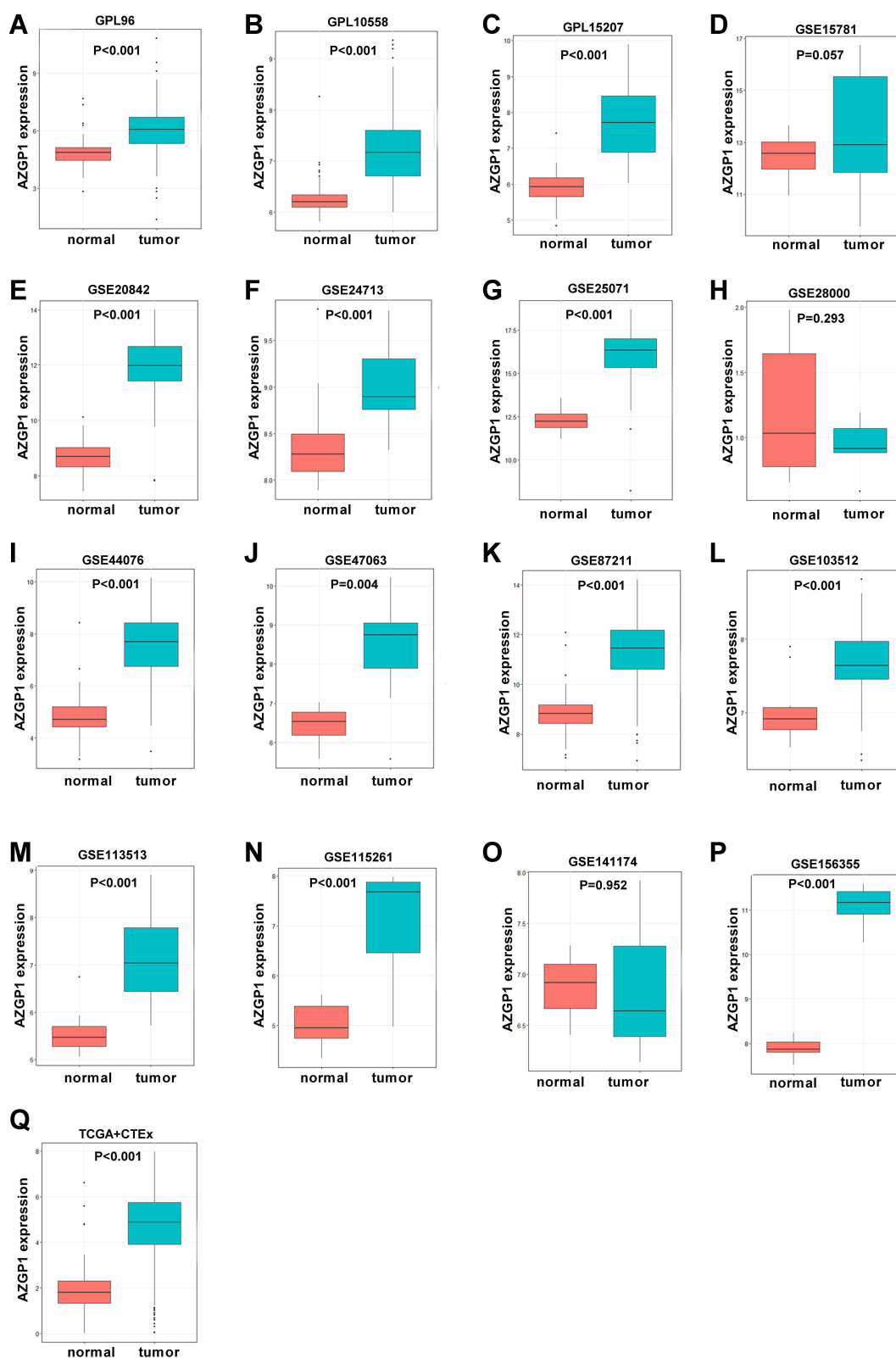


Figure 6 Boxplot of the differentiated expression of AZGP1 in CRC tissue and normal colorectal tissue. (A) GPL96; (B) GPL10558; (C) GPL15207; (D) GSE15781; (E) GSE20842; (F) GSE24713; (G) GSE25071; (H) GSE28000; (I) GSE44076; (J) GSE47063 dataset; (K) GSE87211 dataset; (L) GSE103512 dataset; (M) GSE113513 dataset; (N) GSE115261 dataset; (O) GSE141174 dataset; (P) GSE156355 dataset; (Q) TCGA+CTEx. TCGA, The Cancer Genome Atlas. The Orange boxes represent the expression of AZGP1 in normal colorectal tissue, while the turquoise boxes represent the expression of AZGP1 in CRC tissue.

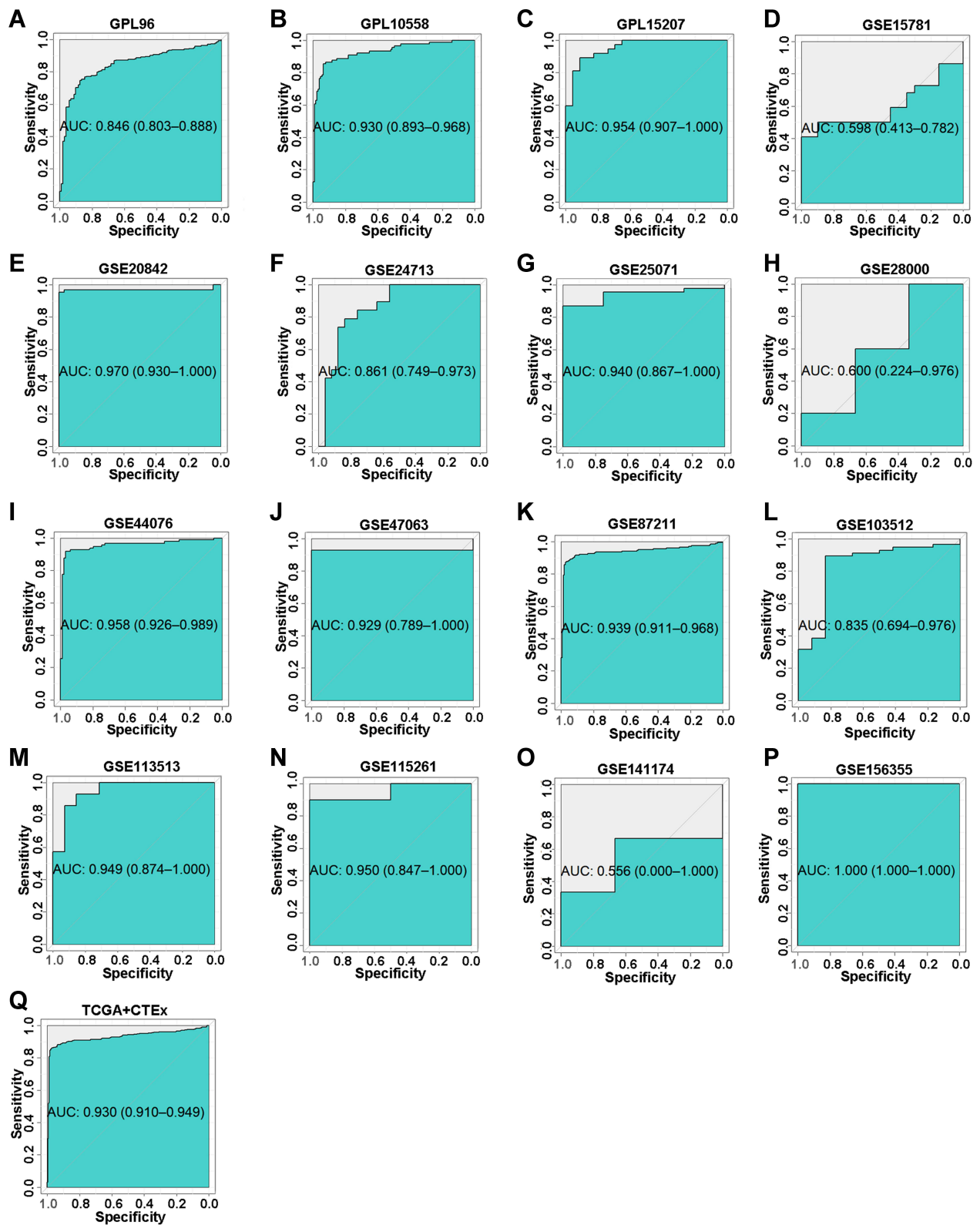


Figure 7 The corresponding ROC curves of AZGPI differential expression in CRC tissue versus normal colorectal tissue. (A) GPL96; (B) GPL10558; (C) GPL15207; (D) GSE15781 dataset; (E) GSE20842; (F) GSE24713; (G) GSE25071; (H) GSE28000; (I) GSE44076; (J) GSE47063; (K) GSE87211; (L) GSE103512; (M) GSE113513; (N) GSE115261; (O) GSE141174; (P) GSE156355; (Q) TCGA+CTEx. TCGA, The Cancer Genome Atlas.

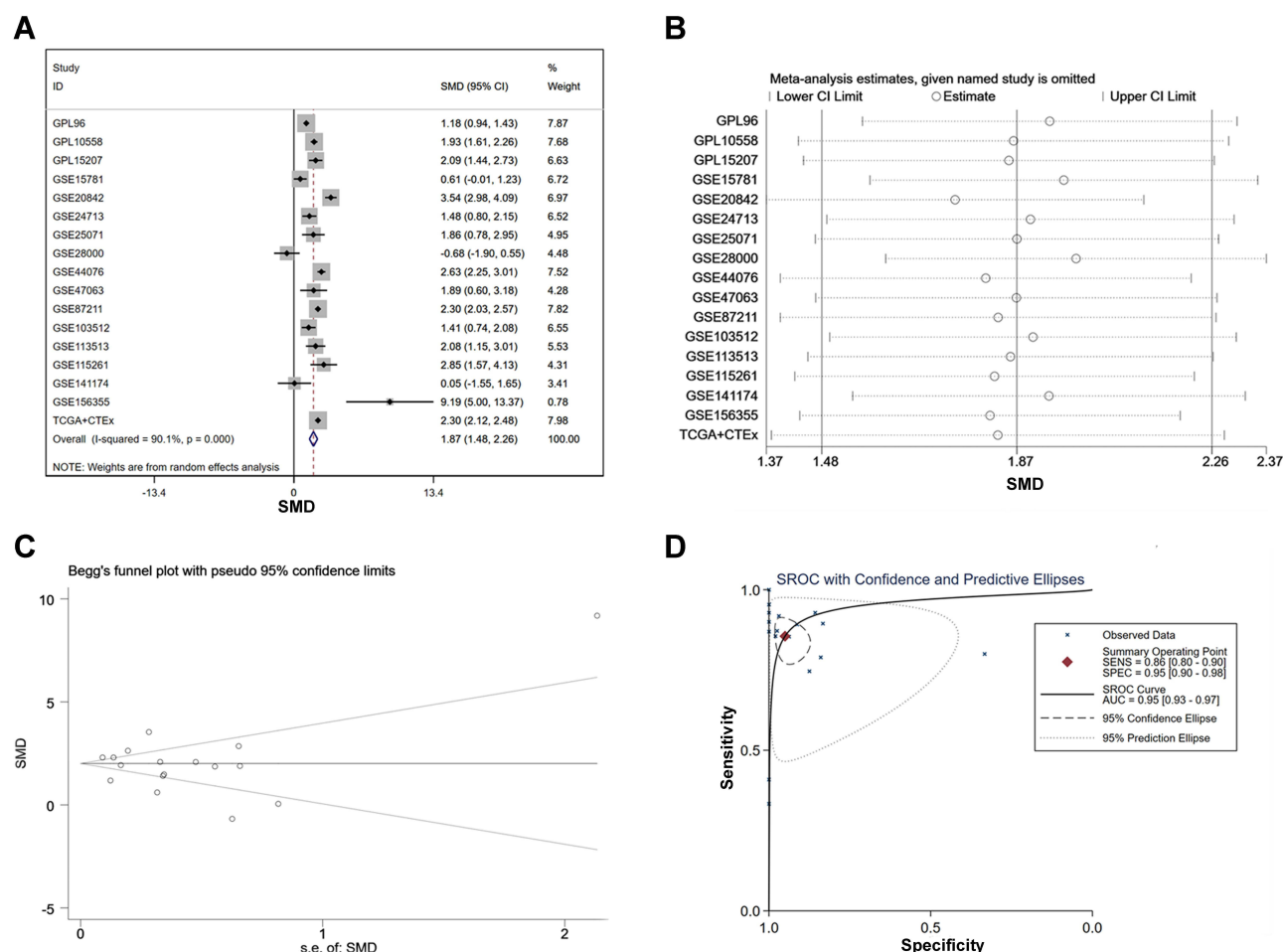


Figure 8 The integrated SMD and diagnostic meta-analysis of AZGP1 expression in CRC tissue versus normal colorectal tissue. **(A)** forest plots of SMD values; **(B)** forest plot of sensitivity analysis; **(C)** funnel plot; **(D)** SROC curve of the included studies.

outcomes. In the present study, we established two acquired radioresistant cell lines, which were derived from radio-sensitive cell line HCT-116 and relatively radioresistant cell line CX-1. Thus, the overlapping differential expression profile not only reflects the intrinsic driving force of radiation resistance, but also the crucial genes involved in the acquired radiation resistance. Another approach to identifying the pivotal genes in radiation resistance is batch data processing, which integrates expression profiles from different detecting platforms and provides more persuasive evidence. For example, our team screened out the crucial driving genes in hepatic carcinoma by analyzing expression profiles from different detecting platforms in batches.^{29,30} Using pooled SMD recalculation, the differentially expressed genes in radioresistant and radiosensitive tissues were screened out, and a SMD value of 0.268 indicated that AZGP1 was upregulated in radioresistant tissues.

AZGP1 (also known as alpha-2-glycoprotein 1, zinc-binding), located at chromosome 7, is the coding gene of ZAG protein.³¹ Because the organization and nucleotide sequence of AZGP1 is similar to the first four exons of major histocompatibility complex (MHC) I genes, it is involved in multiple physiological processes, including lipolysis,³² glucose metabolism,³³ epilepsy,³⁴ and Alzheimer's disease.³⁵ Moreover, AZGP1 inhibits fibrosis of the kidney and heart induced by chronic kidney disease or heart stress by negatively targeting the TGF β pathway.³⁶ The role of AZGP1 in cancer development has also been investigated by some research teams, and the functions of AZGP1 has varied according to type of malignancy. AZGP1 inhibits the TGF- β pathway and thus suppresses the epithelial-to-mesenchymal transition of hepatocellular carcinoma.³⁷ In addition, AZGP1 inhibits the proliferation, invasion, and migration of HCC and soft-tissue sarcoma.³⁷⁻³⁹ It has also been reported that AZGP1 is negatively correlated with the

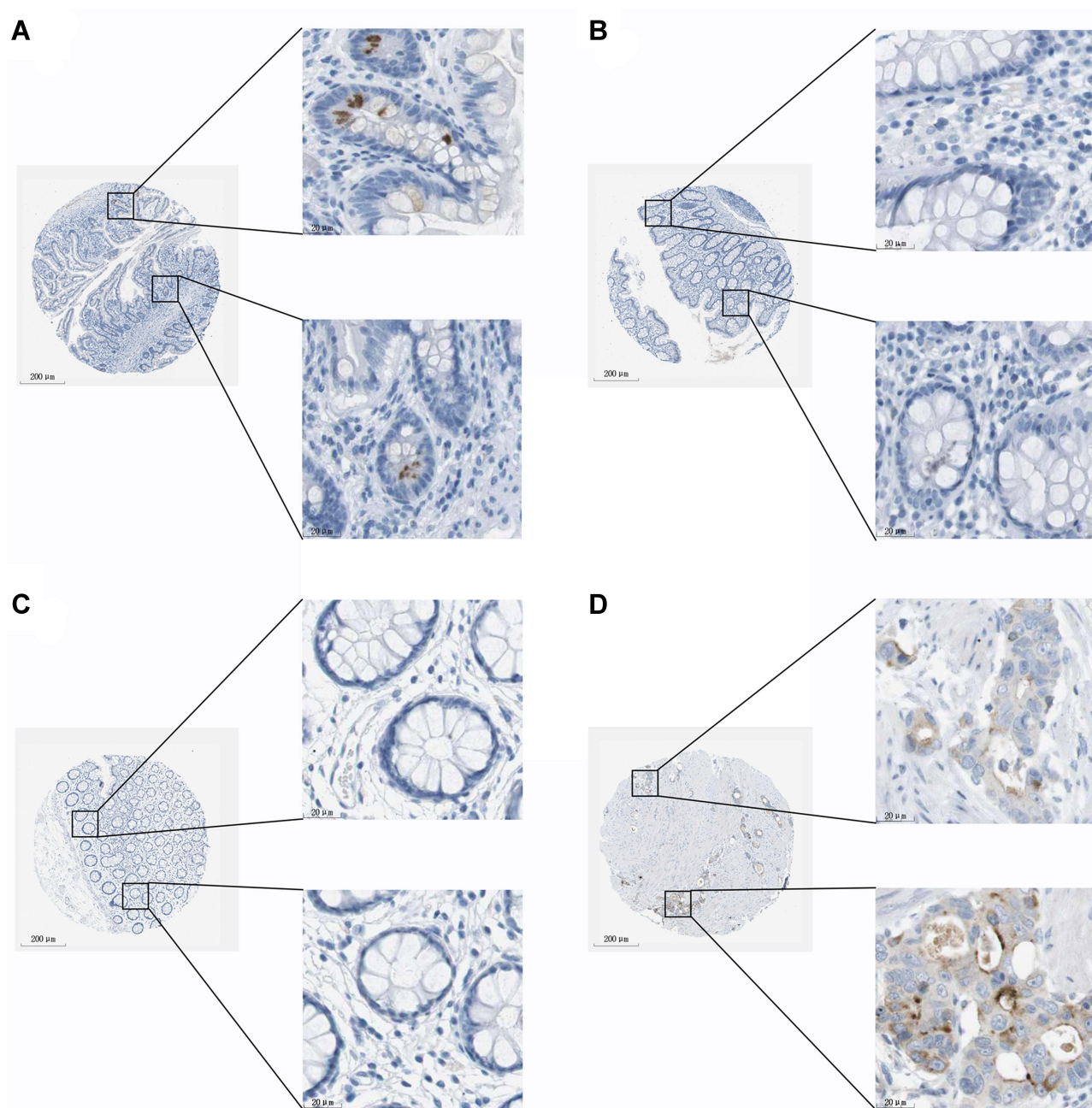


Figure 9 AZGP1 expression in normal tissue and colorectal cancer tissue from the Human Protein Atlas database [antibody CAB016087]. **(A)** Female, age 56. Patient ID 3343. Normal small intestine (T-65000) tissue, NOS(M-00100), low expression of AZGP1. The relative results of glandular cells are as follows: staining: low; intensity: moderate; quantity: <25%; location: cytoplasmic/membranous. **(B)** Female, age 56. Patient ID 1423. Normal colon (T-67000) tissue, NOS(M-0010), deficient expression of AZGP1. The relative results of glandular cells are as follows: staining: not detected; intensity: negative; quantity: none; location: none. **(C)** Female, age 66. Patient ID 2060. Normal rectum (T-68000) tissue, NOS(M-00100), deficient expression of AZGP1. The relative results of glandular cells are as follows: staining: not detected; intensity: negative; quantity: none; location: none. **(D)** Male, age 51. Patient ID 3298. Rectum (T-68000) adenocarcinoma, NOS(M-81403), moderate expression of AZGP1. The relative results of tumor cells are as follows: staining: medium; intensity: moderate; quantity: 75%–25%; location: cytoplasmic/membranous.

prognosis of several malignancies, including soft-tissue sarcoma, esophageal squamous cell carcinoma, and HPV-positive oropharyngeal squamous cell carcinoma.^{39–41} The prognostic value of AZGP1 has been extensively explored in prostate carcinoma, and it has been reported that absent or low AZGP1 expression was not only an independent predictor of biochemical relapse after radical prostatectomy, but also related to increased mortality in several cohort studies.^{42–44} The function of AZGP1 in colorectal carcinoma remains controversial. Yu et al reported that AZGP1 suppresses the proliferation, invasion, and migration of colorectal SW480 cells by upregulating FASN expression.⁴⁵ However, another

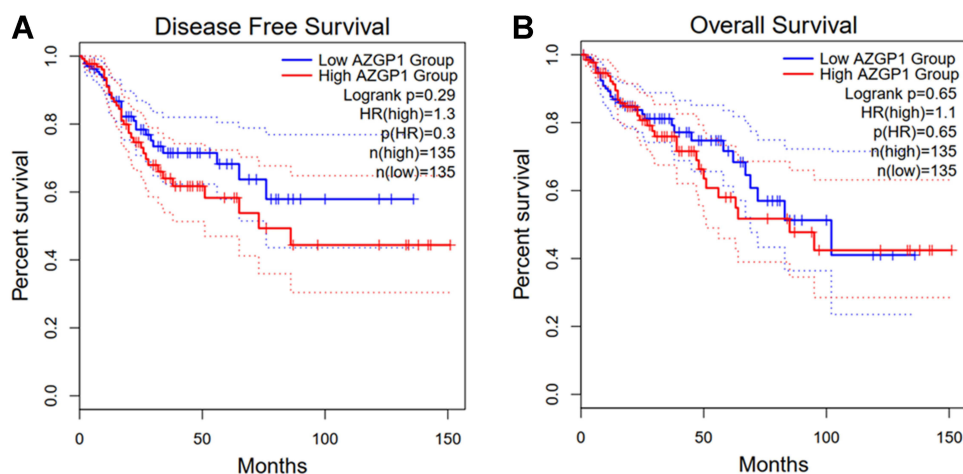


Figure 10 Survival analysis in patients with CRC in terms of disease-free survival and overall survival. (A) Kaplan-Meier curves for disease-free survival; (B) Kaplan-Meier curves for overall survival.

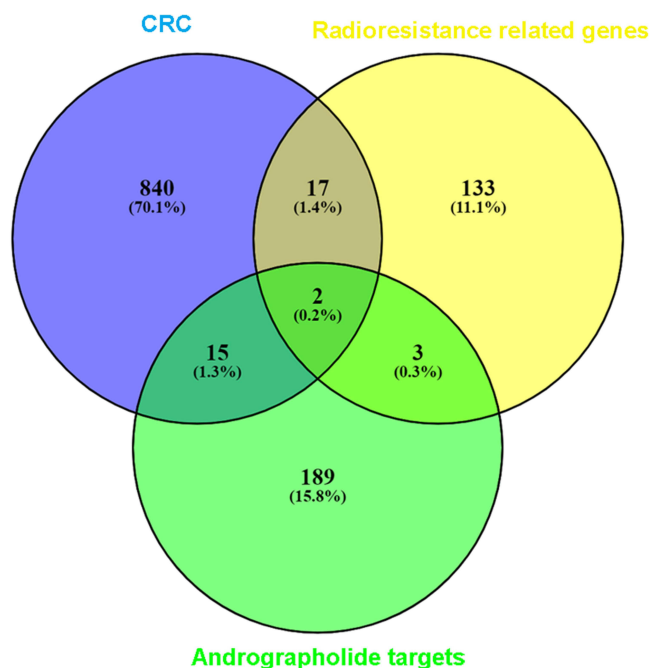


Figure 11 Venn diagrams for the intersections between genes acting on andrographolide and radiotherapy-resistance related genes in colorectal cancer. The 209 andrographolide targets from the different databases and text mining, and the overlapping targets were AZGP1 and SULT2B1.

team observed that AZGP1 was highly expressed in colorectal cancer tissue with liver metastasis and associated with unfavorable survival, and that AZGP1 facilitates metastasis by regulating the epithelial-mesenchymal transition.⁴⁶ In our study, the expression of AZGP1 was upregulated both in HCT-116-R and CX-1-R cells, suggesting its participation in the acquisition of radioresistance. Subsequently, the microarray data from GEO validated the upregulation of AZGP1 in both radioresistant cells and tissues. Contrary to the findings of Yu et al, we found that AZGP1 functions as an oncogene, since patients with low AZGP1 expression enjoyed a more favorable disease-free survival rate, though the influence of AZGP1 on the overall survival of CRC patients was not statistically significant. It may be that the long-term survival of patients with malignancy was actually affected by multiple factors, including age, sex, treatment strategy, and so on, and that the effect of AZGP1 was masked by other more predominant parameters. In other words, AZGP1 was among the factors affecting the prognosis, but not the sole one or the most crucial factor.

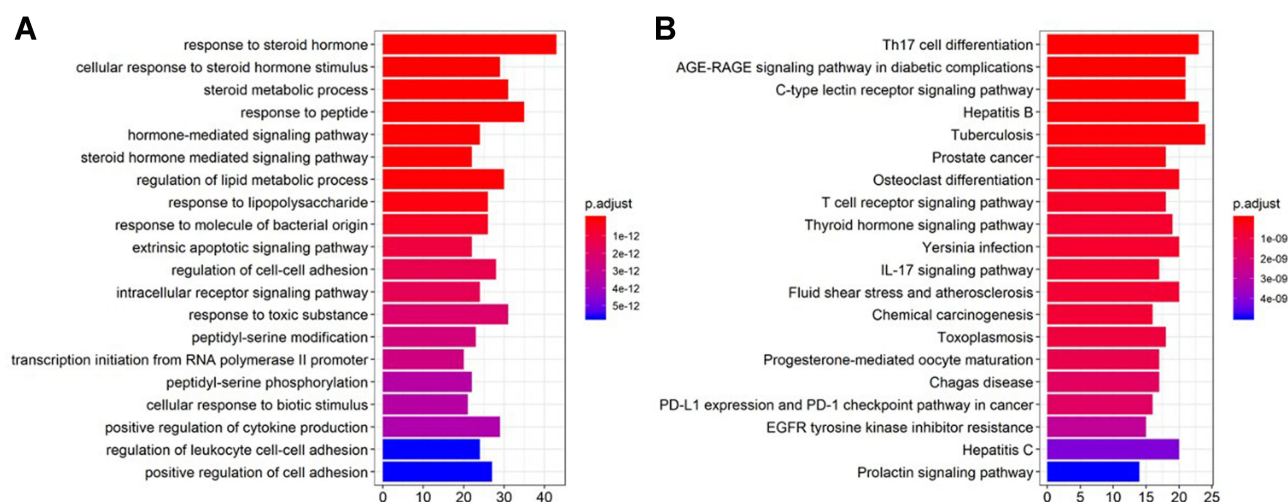


Figure 12 Gene ontology (GO) enrichment and KEGG pathway annotations of the 209 genes related to andrographolide. **(A)** histogram of GO enrichment; **(B)** histogram of GO enrichment of KEGG pathway. The GO analysis was conducted using R package cluster Profiler and visualized using R package GOplot.

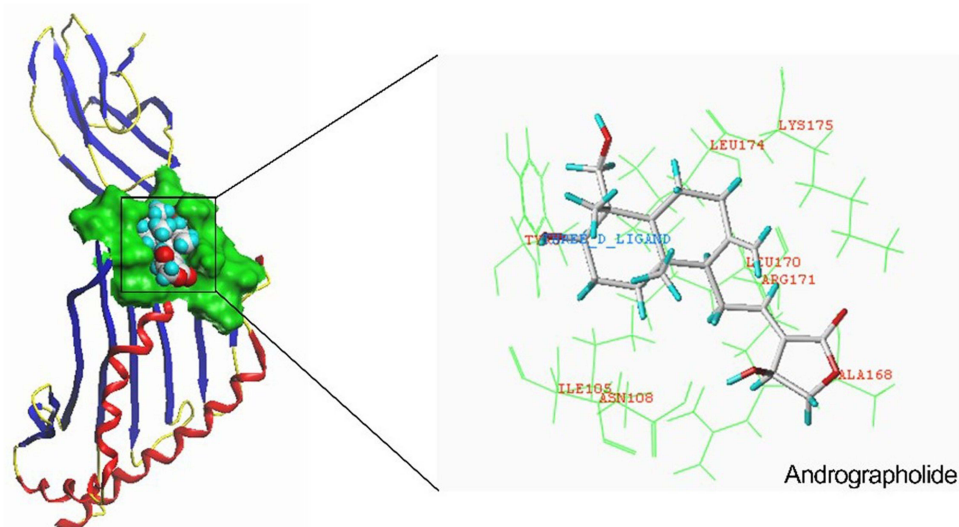


Figure 13 Molecular docking of andrographolide with AZGP1. Schematic diagram of binding of andrographolide with AZGP1 (total score = 7.0941).

One interesting phenomenon is that the SMD value of AZGP1 between cancerous and normal tissues was larger than that between radiosensitive and radioresistant samples. A potential explanation is that AZGP1 is more capable of distinguishing cancerous tissue from non-cancerous tissue, in comparison to its ability to distinguish between radioresistant and radiosensitive samples. In other words, the role of AZGP1 in CRC initiation is more critical than its role in the development of radioresistance. The AUC values of the ROCs in Figure 7 were generally larger than those in Figure 5, further confirming this discrepancy. However, uncovering the exact role and action mechanism of AZGP1 in CRC occurrence, development, and radiation resistance requires more sophisticated experimentation.

The development of network pharmacology has gradually revealed the pharmacological mechanisms underlying a range of traditional Chinese medicine and promoting the popularization and application of traditional Chinese medicine in clinical practice. Andrographolide is the major bioactive component isolated from the plant *Andrographis paniculata* and possesses multiple biological activities, including anti-bacterial, anti-inflammation, anti-virus, anti-fibrosis, anti-obesity, immunomodulatory, and hypoglycemic activities.⁴⁷ The role of andrographolide as an anticarcinogen has been widely studied in the past decade. It has been reported that andrographolide impedes the initiation and development of various malignancies, including colorectal

carcinoma,^{11–13,48,49} gastric cancer,⁵⁰ acute lymphoblastic leukemia,⁵¹ lymphoma,⁵² prostate cancer,⁵³ non-small cell lung cancer,⁵⁴ breast cancer,^{15,55} HCC,⁵⁶ oral squamous cell cancer,⁵⁷ and multiple myeloma.⁵⁸ However, because andrographolide can be rapidly transformed into 14-deoxy-12-sulfo-andrographolide and has low aqueous solubility, its bioavailability is low.⁵⁹ Thus, the application of andrographolide as a sole therapy is of low efficiency and has not been widely used in clinic; the combination of andrographolide with other treatments might to some extent improve its effectiveness. In fact, andrographolide could function as a sensitizer to chemotherapy or radiotherapy. For instance, in one study, andrographolide attenuated autophagy, and therefore alleviated the resistance of A549 cells to cisplatin and paclitaxel *in vitro* and *in vivo*.^{20,60} Andrographolide also reversed both acquired and intrinsic resistance of colorectal cell lines to 5-FU.^{18,19} The synergistic effect of andrographolide on radiation has also been reported, but relatively less is known about it. Wang et al found that andrographolide sensitizes human esophageal cancer cell line ECA109 to radiation *in vitro* by enhancing cellular apoptosis.⁶¹ The combination of andrographolide and radiation in CRC was reported, but only by one team. Li et al investigated the effect of andrographolide on the radio-sensitivity of HCT-116 cells and found that the combination of andrographolide and irradiation increased the response of HCT-116 cells to radiation compared with irradiation alone.²¹ In addition, inactivity of the PI3K-Akt-mTOR signaling pathway was observed upon the administration of andrographolide.²¹ Though their study revealed the potential of andrographolide in radiation sensitization, the usage of a single cell line failed to reflect the profound mechanism underlying radiation resistance. In this study, we used high-throughput sequencing to screen out the differentially expressed genes in the acquired radioresistant cell model, which could more comprehensively demonstrate the major driving force of radiation resistance. Interestingly, AZGP1 is not only a crucial gene in CRC initiation and radioresistance, but also the target of andrographolide. Based on molecular docking, the crystal texture of andrographolide closely intertwines with the protein structure of AZGP1, indicating that andrographolide might inhibit the development or reverse the radioresistance of CRC by targeting AZGP1, a possibility that needs further, more elaborate experiments to elucidate.

This study has some shortcomings. First, some of the findings were based on *in silico* analysis, which occasionally did not fully reflect the nature of radiation resistance. Second, though the results indicated that AZGP1 participates in CRC initiation and radioresistance, the lack of real-world clinical samples of CRC patients undergoing radiotherapy weaken the conclusion. Also, the synergistic effect of andrographolide on radiation was preliminarily investigated, but more sophisticated experiments involving andrographolide and AZGP1 intervention should be conducted to further elucidate whether andrographolide can reverse radiation resistance in CRC by directly targeting AZGP1.

Conclusion

In this study, by establishing the acquired radioresistant cell lines and performing the SMD recomputing, AZGP1 was recognized as a crucial factor for both CRC initiation and radioresistance. Andrographolide may reduce the radio-resistance of CRC by targeting AZGP1. Thus, the combination of andrographolide and AZGP1 intervention might be a promising strategy for improving the treatment benefits of CRC radiotherapy.

Ethics Statement

No human participants or animals were involved in this study, Ethics Committee of the First Affiliated Hospital of Guangxi Medical University waived the requirements for ethics approval.

Acknowledgments

The authors thank the technical support of Guangxi Key Laboratory of Medical Pathology. The authors also thank all of the public databases for the data sources.

Funding

This work was kindly supported by Guangxi Medical High-level Key Talents Training “139” Program (2020), Guangxi Educational Science Planning Key Project (2021B167), Guangxi Higher Education Undergraduate Teaching Reform Project (2021JGA142), and Guangxi Zhuang Autonomous Region Health Commission Self-Financed Scientific Research Project (Z20201186, Z20210442, Z20190406).

Disclosure

The authors declare that they have no conflicts of interest.

References

- Bray F, Ferlay J, Soerjomataram I, Siegel RL, Torre LA, Jemal A. Global cancer statistics 2018: GLOBOCAN estimates of incidence and mortality worldwide for 36 cancers in 185 countries. *CA Cancer J Clin*. 2018;68(6):394–424. doi:10.3322/caac.21492
- Smith CA, Kachnic LA. Evolving treatment paradigm in the treatment of locally advanced rectal cancer. *J Natl Compr Canc Netw*. 2018;16(7):909–915. doi:10.6004/jncn.2018.7032
- Nacion AJD, Park YY, Kim NK. Contemporary management of locally advanced rectal cancer: resolving issues, controversies and shifting paradigms. *Chin J Cancer Res*. 2018;30(1):131–146. doi:10.21147/j.issn.1000-9604.2018.01.14
- Benson AB, Venook AP, Al-Hawary MM, et al. Rectal cancer, version 2.2018, NCCN clinical practice guidelines in oncology. *J Natl Compr Canc Netw*. 2018;16(7):874–901. doi:10.6004/jncn.2018.0061
- Cabrera-Licona A, Perez-Anorve IX, Flores-Fortis M, et al. Deciphering the epigenetic network in cancer radioresistance. *Radiother Oncol*. 2021;159:48–59. doi:10.1016/j.radonc.2021.03.012
- Boeckman HJ, Trego KS, Turchi JJ. Cisplatin sensitizes cancer cells to ionizing radiation via inhibition of nonhomologous end joining. *Mol Cancer Res*. 2005;3(5):277–285. doi:10.1158/1541-7786.MCR-04-0032
- Page P, Yang LX. Novel chemoradiosensitizers for cancer therapy. *Anticancer Res*. 2010;30(9):3675–3682.
- Arcangeli S, Jereczek-Fossa BA, Alongi F, et al. Combination of novel systemic agents and radiotherapy for solid tumors - Part II: an AIRO (Italian association of radiotherapy and clinical oncology) overview focused on treatment toxicity. *Crit Rev Oncol Hematol*. 2019;134:104–119. doi:10.1016/j.critrevonc.2018.11.006
- Wang S, Long S, Wu W. Application of traditional Chinese medicines as personalized therapy in human cancers. *Am J Chin Med*. 2018;46(5):953–970. doi:10.1142/S0192415X18500507
- Kandanur SGS, Tamang N, Golakoti NR, Nanduri S. Andrographolide: a natural product template for the generation of structurally and biologically diverse diterpenes. *Eur J Med Chem*. 2019;176:513–533. doi:10.1016/j.ejmech.2019.05.022
- Khan I, Mahfooz S, Ansari IA. Antiproliferative and Apoptotic Properties of Andrographolide Against Human Colon Cancer DLD1 Cell Line. *Endocr Metab Immune Disord Drug Targets*. 2020;20(6):930–942. doi:10.2174/1871530319666191125111920
- Khan I, Mahfooz S, Faisal M, Alatar AA, Ansari IA. Andrographolide induces apoptosis and cell cycle arrest through inhibition of aberrant hedgehog signaling pathway in colon cancer cells. *Nutr Cancer*. 2020;73:1–19.
- Yuan M, Meng W, Liao W, Lian S. Andrographolide antagonizes TNF- α -induced IL-8 via inhibition of NADPH Oxidase/ROS/NF- κ B and Src/MAPKs/AP-1 axis in human colorectal cancer HCT116 cells. *J Agric Food Chem*. 2018;66(20):5139–5148. doi:10.1021/acs.jafc.8b00810
- Luo W, Jia L, Zhang JW, Wang DJ, Ren Q, Zhang W. Andrographolide against lung cancer-new pharmacological insights based on high-throughput metabolomics analysis combined with network pharmacology. *Front Pharmacol*. 2021;12:596652. doi:10.3389/fphar.2021.596652
- Peng Y, Wang Y, Tang N, et al. Andrographolide inhibits breast cancer through suppressing COX-2 expression and angiogenesis via inactivation of p300 signaling and VEGF pathway. *J Exp Clin Cancer Res*. 2018;37(1):248. doi:10.1186/s13046-018-0926-9
- Li J, Zhang C, Jiang H, Cheng J. Andrographolide inhibits hypoxia-inducible factor-1 through phosphatidylinositol 3-kinase/AKT pathway and suppresses breast cancer growth. *Oncotargets Ther*. 2015;8:427–435. doi:10.2147/OTT.S76116
- Mao W, He P, Wang W, Wu X, Wei C. Andrographolide sensitizes Hep-2 human laryngeal cancer cells to carboplatin-induced apoptosis by increasing reactive oxygen species levels. *Anticancer Drugs*. 2019;30(7):e0774. doi:10.1097/CAD.0000000000000774
- Su M, Qin B, Liu F, Chen Y, Zhang R. Andrographolide enhanced 5-fluorouracil-induced antitumor effect in colorectal cancer via inhibition of c-MET pathway. *Drug Des Devel Ther*. 2017;11:3333–3341. doi:10.2147/DDDT.S140354
- Wang W, Guo W, Li L, et al. Andrographolide reversed 5-FU resistance in human colorectal cancer by elevating BAX expression. *Biochem Pharmacol*. 2016;121:8–17. doi:10.1016/j.bcp.2016.09.024
- Yuwen D, Mi S, Ma Y, et al. Andrographolide enhances cisplatin-mediated anticancer effects in lung cancer cells through blockade of autophagy. *Anticancer Drugs*. 2017;28(9):967–976. doi:10.1097/CAD.0000000000000537
- Li X, Tian R, Liu L, et al. Andrographolide enhanced radiosensitivity by downregulating glycolysis via the inhibition of the PI3K-Akt-mTOR signaling pathway in HCT116 colorectal cancer cells. *J Int Med Res*. 2020;48(8):300060520946169. doi:10.1177/0300060520946169
- Barrett T, Wilhite SE, Ledoux P, et al. NCBI GEO: archive for functional genomics data sets--update. *Nucleic Acids Res*. 2013;41(Database issue):D991–D995. doi:10.1093/nar/gks1193
- Athar A, Fullgrabe A, George N, et al. ArrayExpress update - from bulk to single-cell expression data. *Nucleic Acids Res*. 2019;47(D1):D711–D715. doi:10.1093/nar/gky964
- Leek JT, Johnson WE, Parker HS, Jaffe AE, Storey JD. The sva package for removing batch effects and other unwanted variation in high-throughput experiments. *Bioinformatics*. 2012;28(6):882–883. doi:10.1093/bioinformatics/bts034
- Sjostedt E, Zhong W, Fagerberg L, et al. An atlas of the protein-coding genes in the human, pig, and mouse brain. *Science*. 2020;367:6482. doi:10.1126/science.aay5947
- Tang Z, Li C, Kang B, Gao G, Li C, Zhang Z. GEPIA: a web server for cancer and normal gene expression profiling and interactive analyses. *Nucleic Acids Res*. 2017;45(W1):W98–W102. doi:10.1093/nar/gkx247
- Ru J, Li P, Wang J, et al. TCMSP: a database of systems pharmacology for drug discovery from herbal medicines. *J Cheminform*. 2014;6:13. doi:10.1186/1758-2946-6-13
- Smith JJ, Strombom P, Chow OS, et al. Assessment of a watch-and-wait strategy for rectal cancer in patients with a complete response after neoadjuvant therapy. *JAMA Oncol*. 2019;5(4):e185896. doi:10.1001/jamaoncol.2018.5896
- He RQ, Li JD, Du XF, et al. LPCAT1 overexpression promotes the progression of hepatocellular carcinoma. *Cancer Cell Int*. 2021;21(1):442. doi:10.1186/s12935-021-02130-4
- Huang WJ, He WY, Li JD, et al. Clinical significance and molecular mechanism of angiotensin-converting enzyme 2 in hepatocellular carcinoma tissues. *Bioengineered*. 2021;12(1):4054–4069. doi:10.1080/21655979.2021.1952791

31. Freije JP, Fueyo A, Uria JA, et al. Human Zn-alpha 2-glycoprotein: complete genomic sequence, identification of a related pseudogene and relationship to class I major histocompatibility complex genes. *Genomics*. 1993;18(3):575–587. doi:10.1016/S0888-7543(05)80359-3
32. Xiao X, Li H, Qi X, et al. Zinc alpha2 glycoprotein alleviates palmitic acid-induced intracellular lipid accumulation in hepatocytes. *Mol Cell Endocrinol*. 2017;439:155–164. doi:10.1016/j.mce.2016.06.003
33. Tian M, Liang Z, Liu R, et al. Effects of sitagliptin on circulating zinc-alpha2-glycoprotein levels in newly diagnosed type 2 diabetes patients: a randomized trial. *Eur J Endocrinol*. 2016;174(2):147–155. doi:10.1530/EJE-15-0637
34. Liu Y, Wang T, Liu X, et al. Neuronal zinc-alpha2-glycoprotein is decreased in temporal lobe epilepsy in patients and rats. *Neuroscience*. 2017;357:56–66. doi:10.1016/j.neuroscience.2017.05.043
35. Hu Y, Hosseini A, Kauwe JS, et al. Identification and validation of novel CSF biomarkers for early stages of Alzheimer's disease. *Proteomics Clin Appl*. 2007;1(11):1373–1384. doi:10.1002/prca.200600999
36. Sorensen-Zender I, Bhayana S, Susnik N, et al. Zinc-alpha2-glycoprotein exerts antifibrotic effects in kidney and heart. *J Am Soc Nephrol*. 2015;26(11):2659–2668. doi:10.1681/ASN.2014050485
37. Xu MY, Chen R, Yu JX, Liu T, Qu Y, Lu LG. AZGP1 suppresses epithelial-to-mesenchymal transition and hepatic carcinogenesis by blocking TGFbeta1-ERK2 pathways. *Cancer Lett*. 2016;374(2):241–249. doi:10.1016/j.canlet.2016.02.025
38. Tian H, Ge C, Zhao F, et al. Downregulation of AZGP1 by Ikaros and histone deacetylase promotes tumor progression through the PTEN/Akt and CD44s pathways in hepatocellular carcinoma. *Carcinogenesis*. 2017;38(2):207–217. doi:10.1093/carcin/bgw125
39. Liu J, Han H, Fan Z, et al. AZGP1 inhibits soft tissue sarcoma cells invasion and migration. *BMC Cancer*. 2018;18(1):89. doi:10.1186/s12885-017-3962-5
40. Tang H, Wu Y, Qin Y, et al. Reduction of AZGP1 predicts poor prognosis in esophageal squamous cell carcinoma patients in Northern China. *Oncotargets Ther*. 2017;10:85–94. doi:10.2147/OTT.S113932
41. Poropatich K, Paunesku T, Zander A, et al. Elemental Zn and its binding protein Zinc-alpha2-Glycoprotein are elevated in HPV-positive oropharyngeal squamous cell carcinoma. *Sci Rep*. 2019;9(1):16965. doi:10.1038/s41598-019-53268-1
42. Bruce HM, Stricker PD, Gupta R, et al. Loss of AZGP1 as a superior predictor of relapse in margin-positive localized prostate cancer. *Prostate*. 2016;76(16):1491–1500. doi:10.1002/pros.23233
43. Brooks JD, Wei W, Pollack JR, et al. Loss of expression of AZGP1 is associated with worse clinical outcomes in a multi-institutional radical prostatectomy cohort. *Prostate*. 2016;76(15):1409–1419. doi:10.1002/pros.23225
44. Burdelski C, Kleinhans S, Kluth M, et al. Reduced AZGP1 expression is an independent predictor of early PSA recurrence and associated with ERG-fusion positive and PTEN deleted prostate cancers. *Int J Cancer*. 2016;138(5):1199–1206. doi:10.1002/ijc.29860
45. Ji M, Li W, He G, et al. Zinc-alpha2-glycoprotein 1 promotes EMT in colorectal cancer by filamin A mediated focal adhesion pathway. *J Cancer*. 2019;10(22):5557–5566. doi:10.7150/jca.35380
46. Yu W, Ling J, Yu H, Du J, Liu T. AZGP1 suppresses the process of colorectal cancer after upregulating FASN expression via mTOR signal pathway. *Gen Physiol Biophys*. 2020;39(3):239–248. doi:10.4149/gpb_2019061
47. Zhang H, Li S, Si Y, Xu H. Andrographolide and its derivatives: current achievements and future perspectives. *Eur J Med Chem*. 2021;224:113710. doi:10.1016/j.ejmech.2021.113710
48. Khan I, Khan F, Farooqui A, Ansari IA. Andrographolide exhibits anticancer potential against human colon cancer cells by inducing cell cycle arrest and programmed cell death via augmentation of intracellular reactive oxygen species level. *Nutr Cancer*. 2018;70(5):787–803. doi:10.1080/01635581.2018.1470649
49. Khan I, Mahfooz S, Saeed M, Ahmad I, Ansari IA. Andrographolide inhibits proliferation of colon cancer SW-480 cells via downregulating notch signaling pathway. *Anticancer Agents Med Chem*. 2021;21(4):487–497. doi:10.2174/1871520620666200717143109
50. Dai L, Wang G, Pan W. Andrographolide inhibits proliferation and metastasis of SGC7901 gastric cancer cells. *Biomed Res Int*. 2017;2017:6242103. doi:10.1155/2017/6242103
51. Yang T, Yao S, Zhang X, Guo Y. Andrographolide inhibits growth of human T-cell acute lymphoblastic leukemia Jurkat cells by downregulation of PI3K/AKT and upregulation of p38 MAPK pathways. *Drug Des Devel Ther*. 2016;10:1389–1397. doi:10.2147/DDDT.S94983
52. Yang S, Evens AM, Prachand S, et al. Mitochondrial-mediated apoptosis in lymphoma cells by the diterpenoid lactone andrographolide, the active component of *Andrographis paniculata*. *Clin Cancer Res*. 2010;16(19):4755–4768. doi:10.1158/1078-0432.CCR-10-0883
53. Mir H, Kapur N, Singh R, Sonpavde G, Lillard JW, Singh S. Andrographolide inhibits prostate cancer by targeting cell cycle regulators, CXCR3 and CXCR7 chemokine receptors. *Cell Cycle*. 2016;15(6):819–826. doi:10.1080/15384101.2016.1148836
54. Lee YC, Lin HH, Hsu CH, Wang CJ, Chiang TA, Chen JH. Inhibitory effects of andrographolide on migration and invasion in human non-small cell lung cancer A549 cells via down-regulation of PI3K/Akt signaling pathway. *Eur J Pharmacol*. 2010;632(1–3):23–32. doi:10.1016/j.ejphar.2010.01.009
55. Banerjee M, Chattopadhyay S, Choudhuri T, et al. Cytotoxicity and cell cycle arrest induced by andrographolide lead to programmed cell death of MDA-MB-231 breast cancer cell line. *J Biomed Sci*. 2016;23:40. doi:10.1186/s12929-016-0257-0
56. Chen W, Feng L, Nie H, Zheng X. Andrographolide induces autophagic cell death in human liver cancer cells through cyclophilin D-mediated mitochondrial permeability transition pore. *Carcinogenesis*. 2012;33(11):2190–2198. doi:10.1093/carcin/bgs264
57. Wang LJ, Zhou X, Wang W, et al. Andrographolide inhibits oral squamous cell carcinogenesis through NF-kappaB inactivation. *J Dent Res*. 2011;90(10):1246–1252. doi:10.1177/0022034511418341
58. Gao H, Wang J. Andrographolide inhibits multiple myeloma cells by inhibiting the TLR4/NF-kappaB signaling pathway. *Mol Med Rep*. 2016;13(2):1827–1832. doi:10.3892/mmr.2015.4703
59. Thingale AD, Shaikh KS, Channekar PR, Galgatte UC, Chaudhari PD, Bothiraja C. Enhanced hepatoprotective activity of andrographolide complexed with a biomaterial. *Drug Deliv*. 2015;22(1):117–124. doi:10.3109/10717544.2013.871602
60. Yuan H, Sun B, Gao F, Lan M. Synergistic anticancer effects of andrographolide and paclitaxel against A549 NSCLC cells. *Pharm Biol*. 2016;54(11):2629–2635. doi:10.1080/13880209.2016.1176056
61. Wang ZM, Kang YH, Yang X, et al. Andrographolide radiosensitizes human esophageal cancer cell line ECA109 to radiation in vitro. *Dis Esophagus*. 2016;29(1):54–61. doi:10.1111/dote.12255

Pharmacogenomics and Personalized Medicine

Dovepress

Publish your work in this journal

Pharmacogenomics and Personalized Medicine is an international, peer-reviewed, open access journal characterizing the influence of genotype on pharmacology leading to the development of personalized treatment programs and individualized drug selection for improved safety, efficacy and sustainability. This journal is indexed on the American Chemical Society's Chemical Abstracts Service (CAS). The manuscript management system is completely online and includes a very quick and fair peer-review system, which is all easy to use. Visit <http://www.dovepress.com/testimonials.php> to read real quotes from published authors.

Submit your manuscript here: <https://www.dovepress.com/pharmacogenomics-and-personalized-medicine-journal>